IEEE Access
Multidisciplinary | Rapid Review | Open Access Journal

Received 31 December 2024, accepted 19 January 2025, date of publication 27 January 2025, date of current version 7 February 2025.

Digital Object Identifier 10.1109/ACCESS.2025.3535472

RESEARCH ARTICLE

Target Detection Using Fused Unidentical Photonics-Based LFM Sub-Band Radar Signals With an Adaptive Feed Forward Network Equalizer

BIKASH NAKARMI[1], (Senior Member, IEEE), S. M. REZWANUL ISLAM[1], (Graduate Student Member, IEEE), HUM NATH PARAJULI[2], (Member, IEEE), IKECHI AUGUSTINE UKAEGBU[2,3], (Senior Member, IEEE), AIGERIM ASHIMBAYEVA[4], (Graduate Student Member, IEEE), CARLO MOLARDI[4], (Senior Member, IEEE), T. D. SUBASH[5], (Senior Member, IEEE), XIANGCHUAN WANG[1], AND SHILONG PAN[1], (Fellow, IEEE)

[1]Key Laboratory of Radar Imaging and Microwave Photonics, Ministry of Education, Nanjing University of Aeronautics and Astronautics, Nanjing 210016, China
[2]Integrated Device Solutions and Nanophotonics Laboratory, School of Engineering and Digital Sciences, Nazarbayev University, 010000 Astana, Kazakhstan
[3]Division of Engineering Technology, The University of West Alabama, Livingston, AL 35470, USA
[4]Department of Electrical and Computer Engineering, School of Engineering and Digital Sciences, Nazarbayev University, 010000 Astana, Kazakhstan
[5]School of Marine Engineering Equipment, Zhejiang Ocean University, Zhoushan, Zhejiang 316000, China

Corresponding authors: Bikash Nakarmi (bikash@nuaa.edu.cn) and Shilong Pan (pans@ieee.org)

This work was supported in part by Nanjing University of Aeronautics and Astronautics under Grant 90YAH21066, in part by the Nazarbayev University Collaborative Research under Grant 11022021CRP1507, in part by the Ministry of Education and Science of the Republic of Kazakhstan under Grant AP14871109, and in part by the Nazarbayev University Faculty Development Competitive Research under Grant 201223FD8806.

ABSTRACT To address the challenges of costly frontend high frequency opto-electronics devices and the requirement of high bandwidth for improved range, resolution several band fusion techniques are proposed in this work. However, conventional band fusion techniques fuse the bands with identical bandwidth and same chirp rates. This paper proposes and experimentally demonstrates sub-bands fusion of photonically generated linear frequency modulated (Ph-LFM) radar signals with unidentical bandwidth and chirp rates using an adaptive, delay-less feed-forward network equalizer (FFNE). We demonstrate this using optical injection in a semiconductor laser to generate Ph-LFM signals at different IEEE X-KA radar sub-bands: 19.25–23.94 GHz and 24.06–28.31 GHz (bandgap 0.12 GHz), 19.69–23.06 GHz and 23.625–27 GHz (bandgap 0.56 GHz), and 8–11.5 GHz and 12.75–17 GHz (bandgap 1.25 GHz). Time-frequency analysis (TFA) was used to obtain sub-bandgap signals of 0.12 GHz, 0.56 GHz, and 1.25 GHz which are coherently fused using the FFNE with a particle swarm optimization (PSO) algorithm to optimize complex-valued weights. The method is evaluated by measuring the range resolution and peak-to-sidelobe level (PSL) in detecting two objects separated by 2 cm and 3 cm. The FFNE achieves significant improvement over 10 dB in PSL and resolves previously unresolvable distances, with maximum range resolutions of 1.8 cm, 2.2 cm, and 2 cm, closely matching theoretical values for full-band LFM signals with bandwidth of 9.06 GHz, 7.31 GHz, and 9 GHz, respectively. Experimental results demonstrate the FFNE's superior performance in enhancing range resolution and PSL in multi-sub-band radar systems compared to scenarios without FFNE.

The associate editor coordinating the review of this manuscript and approving it for publication was Cheng Hu.

INDEX TERMS Sub-band fusion, photonic radar, linear frequency modulation, optical injection, feed-forward equalizer, coherent processing.

I. INTRODUCTION

With the advancement in electronic and photonic technologies, the traditional application areas of radio detection and ranging (radar) systems are rapidly expanding from defense applications to civilian applications such as automotive, industrial, agriculture, bio-medical, and consumer electronics [1], [2], [3], [4]. These application areas demand fine range-Doppler resolution for achieving accurate object detection, precise range measurement, and high-range resolution images. This requires high bandwidth radar signal which is difficult to realize in the electronics domain. Microwave photonic (MWP) techniques have shown the potential to generate all weather-operable and highly stable broadband radar signals with reconfigurable features: center frequency, bandwidth, and chirp rates [5], [6], [7], [8]. Despite these advantages, the photonic-based radar (Ph-radar) system still requires high-frequency electronic frontend components and costly opto-electronic components. Additionally, it is difficult to attain the same output performance with high bandwidth signal generation compared to the generation of the narrowband signal [9], [10]. To overcome these issues, techniques that fuse adjacent sub-bands or bands are seen as a promising solution [11], [12], [13], [14], [15], [16], [17], [18], [19], [20]. The fusion technique integrates multiple collocated narrowband radars operating in nearby sub-bands or bands. This results in reduced cost due to the use of narrowband hardware, utilization of available narrowband radar spectrum, and providing advantages associated with broadband radar signals. The fusion of adjacent sub-bands or bands can be accomplished by applying the phase imbalance compensation (PIC) across the corresponding sub-bands or bands. It is important to correct the phase mismatch by PIC between frequency bands before fusing the bands. In addition, the spectral gap estimation (SGE) technique is required to measure the separation and the alignment of two bands before band fusion. Thus, the fusion of distant bands or sub-bands can be achieved by SGE along with PIC. Several advanced signal processing methods such as the compressed sensing method [11], auto-regressive spectral gap filling [12], and the notched spectrum method [13] have been developed to estimate the missing band. Similarly, methods like MUSIC [14], all-phase fast Fourier transform [15], sub-band parameter optimization [16], and more have been utilized to achieve PIC among the bands while performing band fusion. Utilizing above mentioned techniques, researchers have experimentally demonstrated the fusion of photonically generated narrowband signals in [17], [18], [19], [20], and [21]. These implementations involve fusing the bands generated from the same coherent source and transceiver even though the resolution and PSL results [17], [18], [19] are not up to the mark. By applying other accurate signal processing methods such as all-pole processing in electronic domain, the results can be improved [20], [21]. All these band-fusion techniques are implemented with the sub-bands of identical bandwidth and chirp rates. Hence, in this paper, we propose and experimentally demonstrate a novel band fusion approach for photonically generated LFM signals with unidentical bandwidths and chirp rates. This method integrates time-frequency analysis (TFA) with a feed-forward network-based equalizer (FFNE) for SGE and PIC, respectively. Unlike in conventional real-valued FFNE with delays in optical communication system [22], the proposed FFNE structure is fully connected and delay-less, featuring optimized complex-valued weights using the particle swarm optimization (PSO) algorithm [23].

To demonstrate the proposed method, Ph-LFM signals of different IEEE radar bands with different bandwidths and chirp rates are generated using the optical injection technique. The optical injection technique is based on the principle of the occurrence of redshift phenomenon in a semiconductor laser upon the injection of an external optical beam, demonstrated in our previous research works [24], [25]. The generated sub-bands are used to detect two objects with separation distances of 2 cm and 3 cm. The objects are unresolvable with the sub-bands signal as the range resolution is directly dependent on the radar signal bandwidth, R_resolution = C/2B, where C is the speed of light and B is the bandwidth. Therefore, the proposed TFA method for SGE followed by FFNE for PIC is applied before the sub-band fusion. The fused echo signals are evaluated by calculating the range profiles using a matched filtering method without and with FFNE. In the experiment, FFNE with greater than 4 complex-valued weights along with a PSO swarm size of 15 and iteration length of 15 provides the optimum weights among the sub-bands for PIC. The peak-to-sidelobe level (PSL) power improvement of at least 10.4 dB is achieved for a fused signal with FFNE compared to that without FFNE in the range profile. On range-resolution calculations, range-resolution of 1.8 cm, 2.2 cm, and 2 cm are obtained, which are close to the theoretical range resolutions for full bandwidths: 9.06 GHz, 7.31 GHz, and 9 GHz LFM signals. Further, the results of fused signals are compared with the full band Ph-LFM signal of respective bandwidths. These results of range resolution and PSL indicate that the proposed method is effective in coherent sub-band fusion which subsequently enhances the range-resolution and a PSL in multi-sub-band radar systems.

II. EXPERIMENTAL SETUP

The experimental setup for the proposed sub-bands fusion process of Ph-LFM sub-bands signals with different BW and chirp rates are shown in Fig. 1. The experimental setup consists of a main laser (ML) as a tunable laser (TL: ID Photonics, CoBrite-DX) that has an emission wavelength range from 1525 nm to 1611 nm and an output optical power range from 10 dBm to 16 dBm. The distributed feedback laser

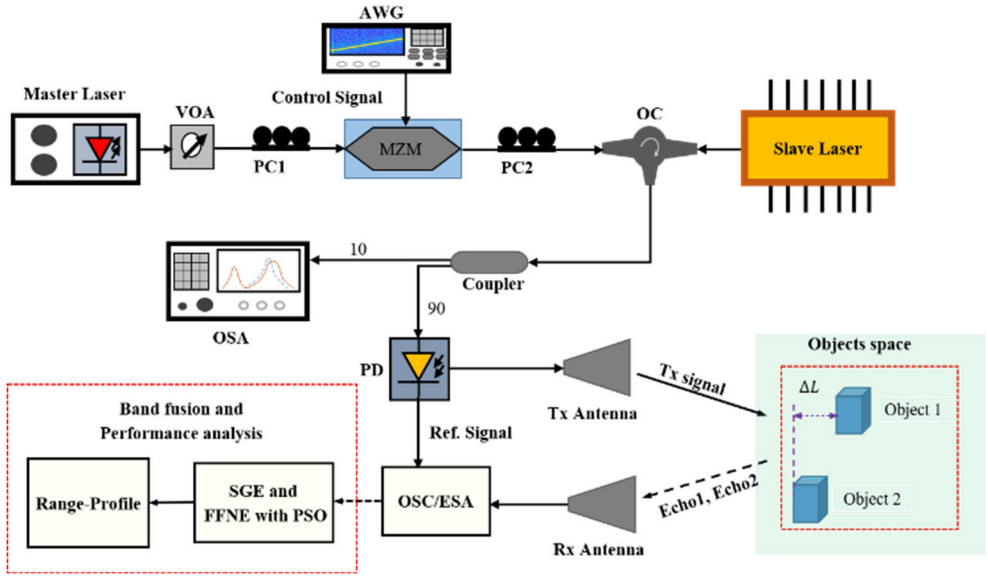

FIGURE 1. Block diagram of the experimental setup.

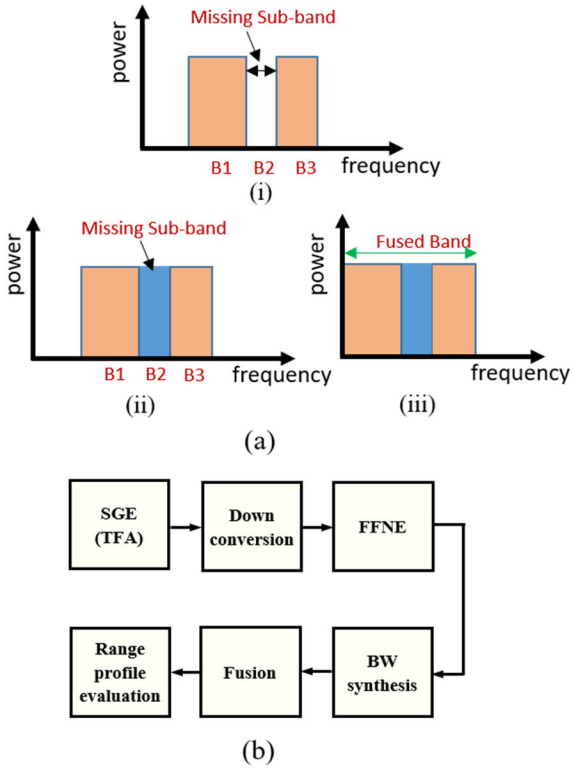

FIGURE 2. Proposed Technique of band-fusion. a) representation of fusion process and b) block diagram of signal processing stages and performance analysis.

(DFB: Actech LD15DM) is a secondary laser (SL), which is biased with a 49 mA driving current and its temperature is stabilized at 21.04° C. At these biasing conditions, SL is operating at 6.77 dBm output power with a wavelength of 1553.28 nm.

When the ML is set to a wavelength of 1553.13 nm for sub-band signal generation, the SL wavelength shifts to 1553.2848 nm resulting in a starting frequency of 19.25 GHz. Similarly, for generating the sub-band signal with a starting frequency of 24.06 GHz, the ML is set to 1553.1 nm. The output power from ML can be adjusted by a variable optical attenuator (VOA). The Mach-Zehnder Modulator (MZM: iXblue, MXAN-LN-20, 20 GHz) is driven by the voltage signal which is generated by a low bandwidth arbitrary waveform generator (AWG: Rigol DG4062, 600 MHz). The polarization controller (PC1) is used to maximize the output power of MZM for the injected optical beam. The circulator helps to inject the light from ML to SL and then deliver the beam to the photodetector. PC2 ensures that the TE polarized light is injected into SL, as it is polarization-dependent. By using ML power of 5.07 dBm and the driving signal from AWG, which is the control signal, in the voltage range of −1.66 V to 2.68 V, the SL wavelength is shifted to 1553.3225 nm. Upon the photodetection, a Ph-LFM RF signal of BW 4.69 GHz is obtained, as discussed in Section IV-A. Unidentical Ph-LFM RF signals (different BW and chirp-rates) are generated by adjusting the AWG control signal which determines the total shift in the emission wavelength of the SL. Using a 90:10 coupler, a 10% output signal is used for the optical signal analysis through the optical spectrum analyzer (OSA: 0.02 nm resolution, Yokogawa AQ6370C), while a 90% signal is applied to the photodetector (PD: u2t-XPDV2120RA). The generated Ph-LFM sub-band signals are amplified and transmitted through the Horn antenna and used to detect two objects spaced 2 cm and 3 cm apart. For 2 cm spacing, the first object is located at a distance of 0.4 m while the second object is placed at 0.42 m from the antenna whereas for 3 cm spacing, only the second object is moved to a distance of 0.43 m from the antenna. In both cases,

the returned echoes are recorded with a real-time oscilloscope (OSC) (Keysight UXR0104B, 33 GHz) and processed offline. Subsequently, the obtained signals are filtered offline using a fourth-order Butterworth bandpass filter. Using the received echoes, TFA-based spectral gap filling is performed to reconstruct the missing sub-band signal between two sub-bands. The three spectral sub-bands are then processed with FFNE and fused. The performance of the proposed method is assessed by analyzing the normalized amplitude in the range profile of the fused signals, with and without FFNE.

III. PRINCIPLES

A. SUB-BANDS FUSION PROCESS OVERVIEW

The basic concept of the proposed sub-band fusion process is illustrated in Fig. 2. The sub-band signals, B1 and B3 are Ph-LFM signals with 1μs time period as well as unidentical bandwidths and chirp rates, are used for detecting two objects in the Objects Space unit as shown in Fig. 1. The received echoes which are reflected from the target objects are used for the sub-bands fusion process. Using the TFA method, the spectral gap filling can be accomplished, as depicted in Fig. 2(a-ii). After the missing band signal (B2) estimation, the down-conversion to baseband, FFNE, and BW synthesis stages are carried out as shown in Fig. 2(b) before the sub-band fusion. The phase and amplitude imbalance among the sub-bands B1, B2, and B3 are corrected with FFNE. The bandwidth synthesis involves frequency shifting operations between the baseband sub-bands, which are required for fusing two echoes with the estimated missing band B2 to achieve full bandwidth as shown in Fig. 2(a-iii). Subsequently, the detection performance is evaluated by calculating the range profile using a cross-correlation technique for both the cases without and with FFNE-based sub-bands fusion signals. The same techniques are repeated for other data sets of sub-bands with different bandwidths, chirp-rates and bandwidth gaps.

B. SUB-BANDS FUSION AND SPECTRAL GAP FILLING

Assume that $x_1(n)$, is the time domain received echo for B1. Taking $x_1(n)$ as a reference signal, the fusion of three sub-bands can be accomplished as

$$\tilde{x}(n) = x_1(n) + \tilde{x}_2(n) + \tilde{x}_3(n) \tag{1}$$

where, $\tilde{x}_2(n)$ and $\tilde{x}_3(n)$ are phase and amplitude imbalance corrected echoes of B2 and B3 sub-bands whose phase and amplitudes are aligned with $x_1(n)$. In this research work, we correct the amplitude and phase mismatch terms by using FFT as in [26]

$$\tilde{X}_2(k) = \Delta a(k) X_2(k) \exp[-1i\Delta\emptyset(k)], \tag{2}$$

where, $X_2(k)$ is the FFT of $x_2(n)$, $\Delta\emptyset(k) = arg[X_1(k)] - arg[X_2(k)]$ is phase imbalance term and $\Delta a(k) = |X_1(k)| - |X_2(k)|$ is amplitude imbalance term between sub-bands B1 and B2. To recover $\tilde{x}_2(n)$, an IFFT operation is carried out to $\tilde{X}_2(k)$, and subsequently used in (1) for the sub-band's fusion. The same procedures are implemented for obtaining $\tilde{x}_3(n)$ as well.

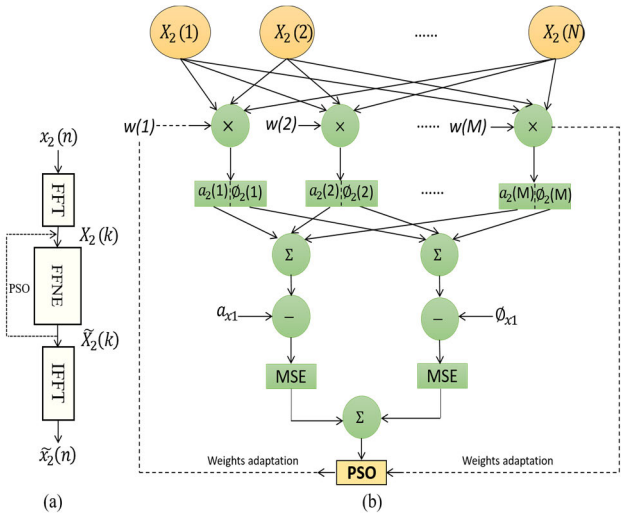

FIGURE 3. FFNE principle and structure with weight adaptation. a) principle and b) structure with PSO-based weights adaptation.

Before sub-band fusion, SGE of the missing sub-band, $x_2(n)$ was obtained. We apply short-time Fourier transform (STFT) and inverse STFT (ISTFT) pairs based TFA method for SGE [27]. For this, we computed the STFT of B1, $X_1(f)$ and B3, $X_3(f)$ and derived the STFT of B2 as

$$X_2(f, i) = X_1(\lfloor a.f + 0.5 \rfloor, i) + X_3(\lfloor b.f + 0.5 \rfloor, i), \tag{3}$$

where, $(f_{c1} + BW_1/2) < f < (f_{c3} - BW_3/2), 1 \le i \le N$, BW_1 and BW_3 are the bandwidths of B1 and B3, and fc_1 and fc_3 are respective center frequencies of B1 and B3. $X_2(f, i)$ represents the elements of the matrix X_2 at frequency index f and time index i, N is the length of the vector, a and b are scaling factors for index and $\lfloor\ \rfloor$ is the floor notation for rounding $a.f$ and $b.f$ to the nearest integers. After SGE as seen in (3), the ISTFT with the windowing operation can be performed to obtain $x_2(n)$. The numerical simulation results of the above analysis can be found in our previous work [28]. To obtain the enhanced resolution, we introduce the FFNE-based method and applied in experimentally generated signals as described in Section III-C.

C. FEED FORWARD NETWORK EQUALIZER (FFNE)

Fig. 3 illustrates the basic principle of the proposed FFNE. As seen in Fig. 3(a), $X_2(k)$ is the input to FFNE, which is the FFT of $x_2(n)$, where, $1 \le k \le N$, and N represents the sample length. Optimum weights obtained from the FFNE are applied to the input signal $X_2(k)$, enabling the achievement of the phase and amplitude compensated signal $\tilde{X}_2(k)$. Then, the IFFT operation converts the frequency domain signal $\tilde{X}_2(k)$ to the time domain signal $\tilde{x}_2(n)$. In radar systems, the delay information of the echoes should be preserved. Thus, we designed the FFNE structure, as illustrated in Fig. 3(b), which is distinct from the traditional FFNE structures with delays [22], [29], [30], [31]. As shown in Fig. 3(b), the proposed FFNE structure consists of a weight multiplier in

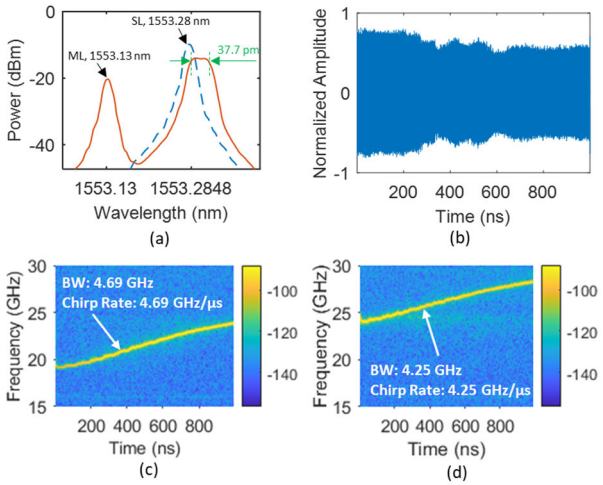

FIGURE 4. Sub-bands generation. a) Optical spectrum associated with Ph-LFM RF signal generation, b) normalized amplitude-time diagram of the photo detected signal, c-d) frequency-time diagrams of data set A: sub-bands Ph-LFM of (19.25 GHz – 23.94 GHz) and (24.06 GHz – 28.31 GHz), respectively.

which each input signal sample is multiplied with weight coefficients $w(m) = w(1), w(2), \ldots, w(M)$, where $1 \leq m \leq M$ and M is the number of weights. The weight $w(m)$, is a complex-valued vector, consisting of phase and amplitude weight terms, given as

$$w(m) = \left[e^{\emptyset(m)} a(m)\right] \tag{4}$$

The weighted output vector can be given as

$$Y(m,k) = \sum_{m=1}^{M} w(m) X_2(k) \tag{5}$$

The amplitude and phase terms for each m can be estimated as described in (2) and subsequently applied to calculate the mean square error (MSE). To handle complex-valued weights, several architectures can be employed, including a simple FFNE structure with two real-valued FFNE [29], [30], [31]. However, the FFNE with two real-valued FFNE structures lags in accuracy for phase estimation and requires larger computational time due to the necessity of adapting two branches of FFNE and hence the optimization algorithm cannot converge at the same time in both branches [30]. To overcome such limitations, we introduce FFNE with a PSO-based optimization algorithm. This approach allows simultaneous processing of amplitude and phase weights within a single FFNE, thereby improving both phase estimation accuracy and computational performance.

The purpose of the FFNE is to obtain the optimum weight vector $w(m)$ which can be applied in (2) to obtain $\tilde{X}_2(k)$. Thus, we design the cost function, J, to include both phase and amplitude correction terms and adapt simultaneously as

$$J = \sum_m \left|\emptyset_1(k) - \emptyset_2(k) \exp\left(-1i\emptyset_2(m)\right)\right|^2 + \sum_m \left|a_1(k) - a_2(k)\, a_2(m)\right|^2 \tag{6}$$

where, $1 \leq \mathrm{m} \leq \mathrm{M}$ and $\emptyset_2(m)$ is the linear phase correction term, $a_2(m)$ is the amplitude correction term, $\emptyset_1(\mathrm{k}) = arg\left[X_1(k)\right]$, $\emptyset_2(\mathrm{k}) = arg\left[X_2(k)\right]$, $a_1(k) = |X_1(k)|$ and $a_2(k) = |X_2(k)|$. The constant phase correction term can be obtained by taking the phase at the index of a maximum value of $a_2(k)$, which represents the constant phase at the center frequency. The constant phase imbalance between sub-bands was compensated before performing FFNE. Thus, the coherency between two sub-bands can be achieved by solving (6) for the optimum minimum value of J. As (6) consists of multiple dissimilar variables $(\emptyset, a)$ that are to be adapted, gradient descent [32], Newton-Raphson methods [33], or PSO algorithms are generally used. Despite the implementation complexity, PSO optimization allows faster convergence and increased accuracy due to its rapid identification of the global optimum solution through its faster search mechanism which is different from other adaptive methods. The faster signal processing is very important for radar applications as real-time or nearly real-time latency is required. Thus, in this manuscript, we implemented the PSO algorithm which not only provides faster convergence but also meets the requirement of complex-valued weights adaptation. The PSO updates the weight parameters as discussed in [23].

$$\Upsilon_\sigma^{q+1}(\emptyset, a) = \Upsilon_\sigma^{q}(\emptyset, a) + \mathrm{u}_\sigma^{q+1}(\emptyset, a) \tag{7}$$

where, σ represents swarm size, q represents iteration length, u is velocity vector, $\Upsilon_\sigma^q(\emptyset, a)$ represents the current value of the particle and $\Upsilon_\sigma^{q+1}(\emptyset, a)$ represents the update vector for the particle at iteration $q+1$ along the dimensions $\emptyset$ and a. The objective is to minimize J using the PSO algorithm, which results in obtaining the optimum values for $w(m)$, as defined by (4). These optimum values serve as phase and amplitude correction factors that can be subsequently used as in (2). While implementing (7), we set the lower and upper bounds for $\emptyset$ and a and their values for each particle are initialized with random values satisfying their respective lower and upper bounds.

IV. RESULTS AND DISCUSSIONS

A. SUB-BAND GENERATION AND FUSION

Fig. 4 illustrates the generation of Ph-LFM signal based on the redshift phenomenon due to optical injection in a semiconductor laser. The optical spectra associated with the Ph-LFM signal generation with the starting frequency of 19.25 GHz is shown in Fig. 4(a). In Fig. 4(a), the dotted blue line and solid orange line refer to the SL spectrum after the circulator without and with the injection of ML, respectively, as depicted in Fig. 1. Before the ML injection, SL is operated at 1553.28 nm with output power of 6.77 dBm. To generate the RF signal at 19.25 GHz starting frequency, the ML is operated at 1553.13 nm. By driving the MZM with the AWG signal of voltage range −1.66 V to 2.68 V, and injecting ML with 5.07 dBm, the SL wavelength is shifted to 1553.3225 nm, as illustrated in Fig. 4(a). Upon the optical beating of shifted SL with ML in a photodetector, the Ph-LFM signal with a bandwidth of 4.69 GHz is generated. Fig. 4(b)

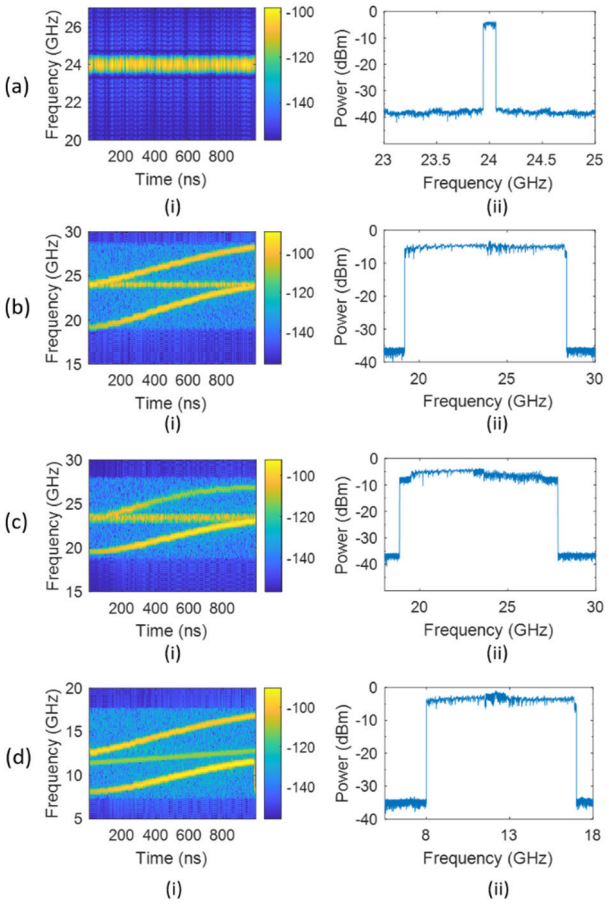

FIGURE 5. Band fusion process. Frequency-time diagram (i) and RF spectrum (ii) of a) estimated missing sub-band signal (23.94 GHz – 24.06 GHz), b) fused signal (19.25 GHz – 28.31 GHz), c) fused signal (19.69 GHz – 27 GHz), d) fused signal (8 GHz – 17 GHz).

shows the normalized amplitude-time diagram of the generated Ph-LFM. Fig.4(c) depicts the frequency-time diagram of the generated sub-band signal with a frequency range of 19.25 GHz – 23.94 GHz. By changing the wavelength and power of the ML, the starting frequency of Ph-LFM signal can be varied and by changing the AWG control signal (amplitude range and the slope of AWG signal) to the modulator, another sub-band LFM signal with the bandwidth 4.25 GHz (24.06 GHz – 28.31 GHz) and chirp rate of 4.25 GHz/us is generated as shown in Fig. 4(d). Similarly, other signals in different radar bands, data set B and C (as shown in Table 1) with different bandwidths, chirp rates, and frequency ranges, such as 3.37 GHz (19.69 GHz – 23.06 GHz) and 3.375 GHz (23.625 GHz – 27 GHz), and 3.5 GHz (8 GHz – 11.5 GHz) and 4.25 GHz (12.75 GHz – 17 GHz), are also generated for band fusion using the same techniques of optical injection. Both these data sets of LFM signals have unidentical bandwidths and the chirp rates which are used to fuse after estimating the bandgap signal using SGE.

In Fig. 5(a-i), the time-frequency diagram of the estimated missing band signal with a bandwidth of

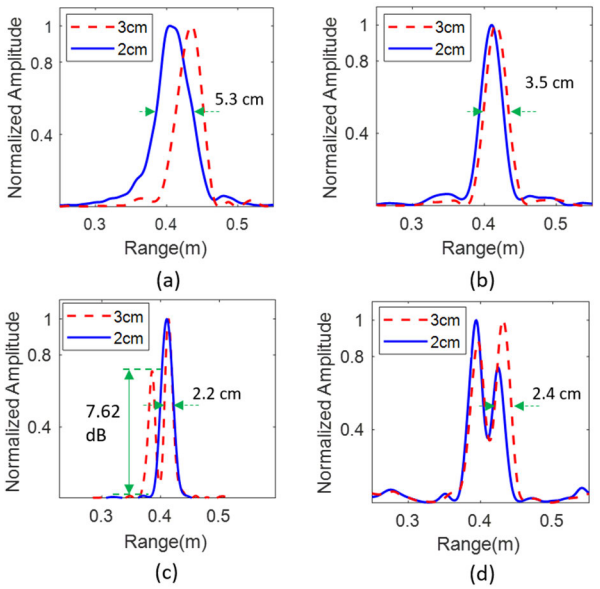

FIGURE 6. Range profiles of detected objects for the signals of a) 4.25 GHz bandwidth, b) 4.69 GHz bandwidth, c) fused signal of 9.06 GHz bandwidth with the SGE of 0.12 GHz and without FFNE, and d) full band Ph-LFM of 9 GHz bandwidth.

0.12 GHz (23.94 GHz–24.06 GHz) using SGE, discussed in Section III-A, is depicted whereas its RF spectrum is shown in Fig. 5(a-ii). The fused signal's time-frequency diagram is shown in Fig. 5(b-i) representing the continuous fusion of three sub-bands. The RF spectrum of the fused signal is shown in Fig. 5(b-ii). To construct the RF spectrum, the fused signal was first filtered with the offline Butterworth band pass filter of order 4 and a roll-off factor of 0.3. Slight uneven flatness is observed in the RF spectrum of the fused bands; however, this uneven flatness does not cause any significant degradation in the obtained results of the FFNE-based range resolution calculations, as described in later in Section IV-C. Further, the time frequency and RF power spectrum of the fused signal for different data set B and C with the bandwidth gap signal estimation of 0.56 GHz and 1.25 GHz are shown in Fig, 5(c) and (d), respectively.

B. OBJECT DETECTION WITHOUT APPLYING FFNE

Fig. 6 shows the range profile of individual, fused signal with band estimation using SGE without FFNE, and full band Ph-LFM for two target objects detection with objects separation distance of 2 cm (blue solid lines) and 3 cm (dotted red lines). Fig. 6(a) depicts the range profiles of the signal with a bandwidth of 4.25 GHz, whereas Fig. 6(b) shows the range profile of the signal with the bandwidth of 4.69 GHz. It is obvious that the two target objects are not resolvable in Fig. 6(a) and (b), since the spacing between them (2 and 3 cm) are less than the theoretical range resolution. In the range profile shown in Fig. 6(b), the linewidth is narrower compared to Fig. 6(a) because it is obtained with a higher bandwidth signal of 4.69 GHz compared to 4.25 GHz.

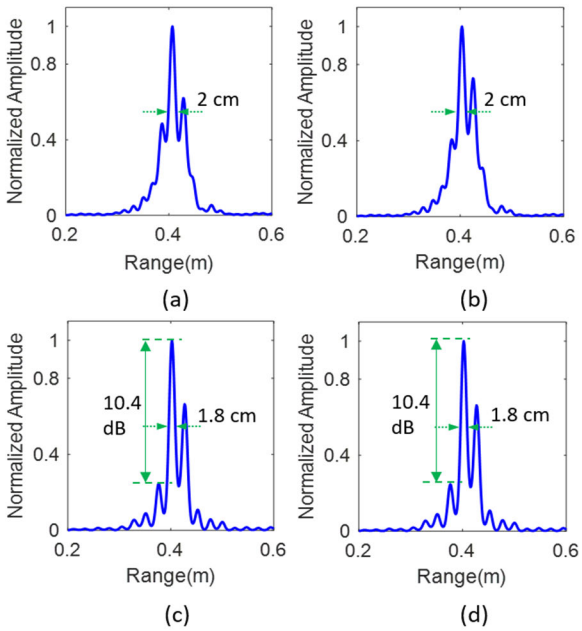

FIGURE 7. Range profiles of detected objects (having 2 cm distance in between) for the band-fused signal of 9.06 GHz bandwidth with a band-gap filling of 0.12 GHz case for the various number of FFNE weights: with a) 1, b) 2, c) 4 and d) 8.

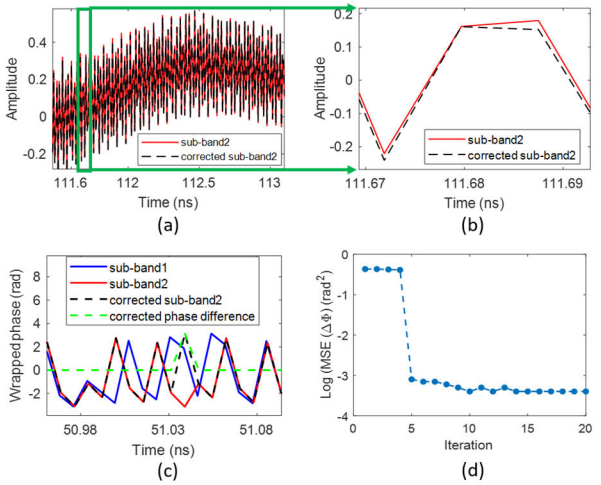

FIGURE 8. Amplitude and phase of sub-band signals and PSO convergence. a) amplitude correction of sub-band2, b) wrapped phases of truncated sub-band signals and c) loss function with respect to iteration.

Similarly, Fig. 6(c) illustrates the range profile of the fused signal obtained from Fig. 5(b), which is the fusion of the two sub-band Ph-LFM signals, Fig. 6(a) and Fig. 6(b), along with the estimated bandgap signal shown in Fig. 5(a). In Fig. 6(c), the target objects with the separation distance of 3 cm are resolved; however, the separation distance of 2 cm is not resolved even though the fused signal has the bandwidth of 9.06 GHz with a theoretical range resolution of 1.66 cm. The inability to resolve the 2 cm separation distance between the target objects is due to the amplitude and phase imbalance among the sub-bands and the estimated band-gap signal [34]. These results show that with fusing the bands, the range resolution can be improved marginally; however, for better resolution, it is necessary to apply advanced methods such as FFNE, which is elaborated in the latter section. In Fig. 6(d), we also show the range profile results using the generated full-band Ph- LFM signal of bandwidth 9 GHz (without band fusion) for comparison, which resolves both the 3 cm and 2 cm separation distances.

C. OBJECT DETECTION WITH APPLYING FFNE

To obtain the optimum values for FFNE and PSO parameters, we evaluate the range resolution and PSL performance of the fused signal of data set A (19.25 GHz - 28.31 GHz) with a 9.06 GHz bandwidth while varying the number of weights. The PSO operating conditions are chosen as swarm size = 15, iteration length = 15, and boundary conditions as [$-\pi$ π] and [0.001 1] for phase and amplitude weights, respectively. The weight vector is initialized randomly within these boundary conditions. In the obtained range profile for target object detections with two objects separated by 2 cm, the objects are not resolvable with one weight FFNE as shown in Fig. 7(a). Whereas, in the case of two weights FFNE, the objects are poorly resolvable as shown in Fig. 7(b). With four weights FFNE, as shown in Fig. 7(c), the objects are resolvable. The PSL and the pulse width at -3 dB are measured as 10.4 dB and 1.8 cm, respectively. The obtained range resolution of 1.8 cm is close to the theoretical range resolution of 1.66 cm for a 9.06 GHz LFM signal. The PSL and range resolution values remain almost similar for cases where M $\geq$4, as illustrated in Fig. 7(d) for eight weights. Thus, the required number of weights is M $\geq$4 for the given signal scenarios and PSO operating conditions.

Fig. 8 illustrates the amplitude-time and phase diagrams of sub-band1, sub-band2, phase corrected sub-band2, and the corrected phase difference denoted by blue, red, dotted black, and green colored lines. Fig. 8(a) depicts the amplitude correction of sub-band2 and Fig. 8(b) shows zoom view of the portion indicated by the deep green rectangular box in Fig. 8(a). Fig. 8(c) expresses wrapped phases of the truncated signals. The phase correction in the range of [$-\pi$ π] radian has been applied. Fig. 8(d) shows the PSO loss function with respect to the PSO iteration length. It illustrates that the PSO converges within an iteration length of less than 15 and the mean square error (MSE) of the phase imbalance value is reduced to $<10^{-3}$. Therefore, the proposed phase correction method with FFNE is effective and has shown reasonable performance, as illustrated in Fig. 7 and described in this subsection.

Further, to illustrate the effectiveness of the proposed FFNE for coherently fusing various unidentical bandwidth, chirp rate, and bandwidth gap of sub-bands signals, we generated the sub-bands data set B and data set C. Data set B has sub-bands B1 with 3.37 GHz bandwidth, B3 with 3.38 GHz bandwidth and chirp rate of 3.38 GHz/μs and a

TABLE 1. Summary of object detection performance.

Data Sets	Signal types	2 cm spacing	3 cm spacing
SET A Bandgap and BW of 0.12 GHz and 9 GHz and different chirp rates	Sub-band1 (19.25-23.94) GHz	Un-resolved	Un-resolved
	Sub-band 3 (24.06-28.31) GHz	Un-resolved	Un-resolved
	Fused (19.25-28.31) GHz with SGE and without FFNE	Un-resolved	Resolution: 2.2 cm PSL: 7.62 dB
	(**Proposed**): Fused (19.25-28.31) GHz with SGE and FFNE	Resolution: 1.8 cm PSL: 10.4 dB	Resolution: 1.8 cm PSL: 10.4 dB
	Full band (19.3-28.3) GHz	Resolution: 2.2 cm PSL: 10.91 dB	Resolution: 2.4 cm PSL: 12.22 dB
SET B Bandgap and BW of 0.56 GHz and 7.3 GHz and different chirp rates	Sub-band1 (19.69-23.06) GHz	Un-resolved	Un-resolved
	Sub-band 3 (23.62-27) GHz	Un-resolved	Un-resolved
	Fused (19.69-27) GHz with SGE without FFNE	Un-resolved	Un-resolved
	(Proposed): Fused (19.69-27) GHz with SGE and FFNE	Un-resolved	Resolution: 2.2 cm PSL: 10.37 dB
	Full band (19.7-27) GHz	Un-resolved	Resolution: 2.5 cm PSL: 10.6 dB
SET C Bandgap and BW of 1.25 GHz and 9 GHz and different chirp rates	Sub-band1 (8-11.5) GHz	Un-resolved	Un-resolved
	Sub-band 3 (12.75-17) GHz	Un-resolved	Un-resolved
	Fused (8-17) GHz with SGE without FFNE	Un-resolved	Resolution: 2.2 cm PSL: 7.58 dB
	(Proposed): Fused (8-17) GHz with SGE and FFNE	Resolution: 2 cm PSL: 10.28 dB	Resolution: 2 cm PSL: 10.28 dB
	Full band (8-17) GHz	Resolution: 2.2 cm PSL: 10.84 dB	Resolution: 2.3 cm PSL: 12.36 dB

bandgap B2 of 0.56 GHz bandwidth. Similarly, data set C has sub-bands B1 with 3.5 GHz bandwidth and chirp rate of 3.5 GHz/μs, B3 with 4.25 GHz bandwidth and chirp rate of 4.25 GHz/μs and bandgap B2 of 1.25 GHz between two sub-bands. With these Ph-LFM signals of different frequency ranges and bandwidths, a range-profile analysis is carried out by detecting two objects spaced 2 cm and 3 cm apart with individual sub bands, fused sub bands with SGE and fused sub bands with both SGE and FFNE which are provided in Table 1 for the comparison. In Table 1, the results show that the band fused signal with FFNE is superior compared to that of without FFNE. The results are closely matched with the results of experimentally generated full band signals (without band gap estimation) of frequency ranges, 19.3 GHz – 28.3 GHz (bandwidth of 9 GHz), 19.7 GHz – 27 GHz (bandwidth of 7.3 GHz), and 8 GHz – 17 GHz (bandwidth of 9 GHz) respectively.

In data set B, the detection of two objects with the separation distance of 2 cm is unresolved for both cases (with FFNE and full band) because the theoretical range resolution of radar signal with 7.3 GHz is 2.05 cm. Whereas for the objects with the separation distance of 3 cm are resolved (which was not the case without proposed FFNE) with better PSL and range resolution as shown in Table 1. The data set C shows the result of the same methods but in relatively lower frequency range, i.e., from 8 GHz to 17 GHz. The results obtained with FFNE-based fusion (PSL $>$ 10 dB) are comparable to those of full band experimental signals (PSL $>$ 10.5 dB). These differences are reasonable because the sub-bands signals experience different noise characteristics, and after fusion, the fused signal can be little nosier compared to the individual full-band signal. Additionally, from the data sets shown in Table 1, it is observed that the proposed technique performs well regardless the bandwidths, chirp rate of the sub band signals, bandwidth of the missing band, and the frequency band of the signals.

V. CONCLUSION

In this paper, we introduced a sub-band fusion technique for Ph-LFM radar signals using complex-valued FFNE-based coherent processing and detect the target object using the fused LFM signals with the range resolution closely matched with the full band LFM signals. Through the experiments, we validate the efficacy of the proposed FFNE-based sub-band fusion method in fusing the sub-bands with unequal bandwidths, unidentical chirp rate signals and different band-gaps in different IEEE radar bands. We initially generated two adjacent sub-band signals using external optical beam injection in a semiconductor laser. Time-frequency analysis (TFA) was employed to estimate the spectral gap signal before applying FFNE for sub-bands fusion. The FFNE, equipped with complex-valued weights optimized via the particle swarm optimization (PSO) algorithm, effectively estimates and compensates for amplitude and phase imbalances between sub-bands, which are subsequently applied to create full band coherent radar signal. The effectiveness of the proposed FFNE with PSO is evaluated by comparing the peak-to-side lobe level (PSL) and the range resolution while detecting two target objects, separated by 2 cm and 3 cm, respectively. With the proposed technique, we achieved a PSL enhancement of $>$10 dB and range resolutions which closely aligns with the theoretical range resolution for respective full band LFM signals. The FFNE is further evaluated with the fusion of sub-bands having dissimilar bandwidths and a bandgap at different frequency range and IEEE radar bands by detecting two target objects separated by 2 cm and 3 cm. The proposed FFNE-based sub-band fusion technique showed superior performance compared to the sub-band fusion without FFNE even with the unidentical bandwidth and chirp rates. Furthermore, the performance of

FFNE-based sub-band fusion was found to be comparable to that of the experimentally generated full band signals in target object detection experiments. This demonstrates the potential of the proposed scheme for application in higher-frequency multiple IEEE radar bands and its possible incorporation into cutting-edge radar technologies or artificial intelligence techniques, which will be explored in future research. With ongoing advancements in digital signal processors (DSP), field programmable gate arrays (FPGA), and graphics processing units (GPU) [35], [36], the proposed FFNE method holds significant promise for practical applications, offering enhanced range resolution and PSL making it well-suited for multi-radar environments.

REFERENCES

[1] C. Waldschmidt, J. Hasch, and W. Menzel, "Automotive radar—From first efforts to future systems," *IEEE J. Microw.*, vol. 1, no. 1, pp. 135–148, Jan. 2021, doi: 10.1109/JMW.2020.3033616.

[2] Y. Eder and Y. C. Eldar, "Sparsity-based multi-person non-contact vital signs monitoring via FMCW radar," *IEEE J. Biomed. Health Informat.*, vol. 27, no. 6, pp. 2806–2817, Jun. 2023, doi: 10.1109/JBHI.2023.3255740.

[3] S. C. Steele-Dunne, H. McNairn, A. Monsivais-Huertero, J. Judge, P.-W. Liu, and K. Papathanassiou, "Radar remote sensing of agricultural canopies: A review," *IEEE J. Sel. Topics Appl. Earth Observ. Remote Sens.*, vol. 10, no. 5, pp. 2249–2273, May 2017, doi: 10.1109/JSTARS.2016.2639043.

[4] W. Wiesbeck and L. Sit, "Radar 2020: The future of radar systems," in *Proc. Int. Radar Conf.*, Oct. 2014, pp. 1–6, doi: 10.1109/RADAR.2014.7060395.

[5] C. Ma, Y. Yang, C. Liu, B. Fan, X. Ye, Y. Zhang, X. Wang, and S. Pan, "Microwave photonic imaging radar with a sub-centimeter-level resolution," *J. Lightw. Technol.*, vol. 38, no. 18, pp. 4948–4954, Jun. 8, 2020, doi: 10.1109/JLT.2020.3000488.

[6] S. Pan and Y. Zhang, "Microwave photonic radars," *J. Lightw. Technol.*, vol. 38, no. 19, pp. 5450–5484, May 7, 2020, doi: 10.1109/JLT.2020.2993166.

[7] B. Nakarmi, B. Y. Song, I. A. Ukaegbu, H. N. Parajuli, A. Ashimbayeva, U. Nakarmi, X. Wang, and S. Pan, "Multi-chirp LFM waveforms generation with reconfigurable chirp rates using optical injection in a semiconductor laser," *J. Lightw. Technol.*, vol. 42, no. 1, pp. 184–193, Aug. 18, 2023, doi: 10.1109/jlt.2023.3306476.

[8] S. Maresca, G. Serafino, C. Noviello, F. Scotti, G. Fornaro, E. Sansosti, A. Bogoni, and P. Ghelfi, "Field trial of a coherent, widely distributed, dual-band photonics-based MIMO radar with ISAR imaging capabilities," *J. Lightw. Technol.*, vol. 40, no. 20, pp. 6626–6635, Jun. 13, 2022, doi: 10.1109/JLT.2022.3182421.

[9] X. Wang, F. Cao, C. Ma, Y. Yang, F. Zhang, and S. Pan, "Dual-band coherent microwave photonic radar using linear frequency modulated signals with arbitrary chirp rates," *IEEE J. Sel. Topics Quantum Electron.*, vol. 29, no. 6, pp. 1–9, Nov. 2023, doi: 10.1109/JSTQE.2023.3272108.

[10] F. Scotti, F. Laghezza, P. Ghelfi, and A. Bogoni, "Multi-band software-defined coherent radar based on a single photonic transceiver," *IEEE Trans. Microw. Theory Techn.*, vol. 63, no. 2, pp. 546–552, Feb. 2015, doi: 10.1109/TMTT.2014.2386877.

[11] S. Guha, A. Bathelt, M. H. Conde, and J. Ender, "Radar band fusion using frame-based compressed sensing," *IEEE J. Sel. Topics Signal Process.*, vol. 17, no. 2, pp. 403–415, Mar. 2023, doi: 10.1109/JSTSP.2022.3220403.

[12] B. Hussain, A. Malacarne, S. Maresca, F. Scotti, P. Ghelfi, and A. Bogoni, "Auto-regressive spectral gap filling algorithms for photonics-based highly sparse coherent multi-band radars in complex scenarios," in *Proc. IEEE Radar Conf.*, Oklahoma City, OK, USA, Apr. 2018, pp. 993–998, doi: 10.1109/RADAR.2018.8378696.

[13] J. Karlsson, W. Rowe, L. Xu, G.-O. Glentis, and J. Li, "Fast missing-data IAA with application to notched spectrum SAR," *IEEE Trans. Aerosp. Electron. Syst.*, vol. 50, no. 2, pp. 959–971, Apr. 2014, doi: 10.1109/TAES.2014.120529.

[14] K. M. Cuomo, J. E. Pion, and J. T. Mayhan, "Ultrawide-band coherent processing," *IEEE Trans. Antennas Propag.*, vol. 47, no. 6, pp. 1094–1107, Jun. 1999, doi: 10.1109/8.777137.

[15] J. Tian, J. Sun, G. Wang, Y. Wang, and W. Tan, "Multiband radar signal coherent fusion processing with IAA and apFFT," *IEEE Signal Process. Lett.*, vol. 20, no. 5, pp. 463–466, May 2013, doi: 10.1109/LSP.2013.2251631.

[16] D. Huang, Y. Zhang, and H. Zhao, "A sub-bands parameter optimization method for frequency multiband fusion based on PSO," *IEEE Antennas Wireless Propag. Lett.*, vol. 24, no. 1, pp. 33–37, Jan. 2025, doi: 10.1109/LAWP.2024.3482311.

[17] F. Scotti, F. Laghezza, A. Bogoni, and D. Onori, "Data fusion in a fully coherent photonics-aided dual-band radar system," in *Proc. Eur. Radar Conf. (EuRAD)*, Paris, France, Sep. 2015, pp. 245–248, doi: 10.1109/EuRAD.2015.7346283.

[18] S. Peng, S. Li, X. Xue, X. Xiao, D. Wu, and X. Zheng, "A photonics-based coherent dual-band radar for super-resolution range profile," *IEEE Photon. J.*, vol. 11, no. 4, pp. 1–8, Aug. 2019, doi: 10.1109/JPHOT.2019.2929210.

[19] P. Ghelfi, F. Laghezza, F. Scotti, D. Onori, and A. Bogoni, "Photonics for radars operating on multiple coherent bands," *J. Lightw. Technol.*, vol. 34, no. 2, pp. 500–507, Sep. 25, 2015, doi: 10.1109/JLT.2015.2482390.

[20] X. Zhu, G. Sun, and F. Zhang, "Photonics-based multiband radar fusion with millimeter-level range resolution," in *Proc. Opt. Fiber Commun. Conf. Exhib. (OFC)*, Mar. 2022, pp. 1–3.

[21] N. Zhong, P. Li, W. Bai, W. Pan, L. Yan, and X. Zou, "Spectral-efficient frequency-division photonic millimeter-wave integrated sensing and communication system using improved sparse LFM sub-bands fusion," *J. Lightw. Technol.*, vol. 41, no. 23, pp. 7105–7114, Apr. 10, 2023, doi: 10.1109/JLT.2023.3265799.

[22] P. M. Watts, V. Mikhailov, S. Savory, P. Bayvel, M. Glick, M. Lobel, B. Christensen, P. Kirkpatrick, S. Shang, and R. I. Killey, "Performance of single-mode fiber links using electronic feed-forward and decision feedback equalizers," *IEEE Photon. Technol. Lett.*, vol. 17, no. 10, pp. 2206–2208, Oct. 2005, doi: 10.1109/LPT.2005.856326.

[23] J. Kennedy and R. Eberhart, "Particle swarm optimization," in *Proc. Int. Conf. Neural Netw.*, vol. 4, 1995, pp. 1942–1948, doi: 10.1109/icnn.1995.488968.

[24] B. Nakarmi, B. Y. Song, H. N. Parajuli, I. A. Ukaegbu, W. Xiangchun, and S. Pan, "Multi-chirp piecewise linearly frequency modulated microwave generation using a semiconductor laser," *IEEE Photon. Technol. Lett.*, vol. 35, no. 15, pp. 821–824, May 31, 2023, doi: 10.1109/LPT.2023.3281640.

[25] H. Chen, P. Zhou, L. Zhang, S. Bassi, B. Nakarmi, and S. Pan, "Reconfigurable identical and complementary chirp dual-LFM signal generation subjected to dual-beam injection in a DFB laser," *J. Lightw. Technol.*, vol. 38, no. 19, pp. 5500–5508, May 8, 2020, doi: 10.1109/JLT.2020.2993368.

[26] M. Sedláček and M. Krumpholc, "Digital measurement of phase difference—A comparative study of DSP algorithms," *Metrol. Meas. Syst.*, vol. 12, pp. 427–448, Jan. 2005.

[27] D. Griffin and J. Lim, "Signal estimation from modified short-time Fourier transform," *IEEE Trans. Acoust., Speech, Signal Process.*, vol. ASSP-32, no. 2, pp. 236–243, Apr. 1984, doi: 10.1109/TASSP.1984.1164317.

[28] H. N. Parajuli, A. Ashimbayeva, B. Nakarmi, and I. A. Ukaegbu, "Enhancing detection performance of multi-band photonic radars through band fusion with coherent processing," in *Proc. Int. Topical Meeting Microw. Photon. (MWP)*, Nanjing, China, Oct. 2023, pp. 1–4, doi: 10.1109/mwp58203.2023.10416566.

[29] C. Farhati, S. Fki, A. A. El Bey, and F. Abdelkefi, "Blind channel equalization based on complex-valued neural network and probability density fitting," in *Proc. Int. Wireless Commun. Mobile Comput. (IWCMC)*, Dubrovnik, Croatia, May 2022, pp. 773–777, doi: 10.1109/IWCMC55113.2022.9824100.

[30] D. Wang, M. Aziz, M. Helaoui, and F. M. Ghannouchi, "Augmented real-valued time-delay neural network for compensation of distortions and impairments in wireless transmitters," *IEEE Trans. Neural Netw. Learn. Syst.*, vol. 30, no. 1, pp. 242–254, Jan. 2019, doi: 10.1109/TNNLS.2018.2838039.

[31] C. Lee, H. Hasegawa, and S. Gao, "Complex-valued neural networks: A comprehensive survey," *IEEE/CAA J. Autom. Sinica*, vol. 9, no. 8, pp. 1406–1426, Aug. 2022, doi: 10.1109/JAS.2022.105743.

[32] S. Boyd and L. Vandenberghe, *Convex Optimization*, 1st ed., Cambridge, U.K.: Cambridge Univ. Press, 2004.

[33] J. Nocedal and S. J. Wright, *Numerical Optimization*, 2nd ed., Berlin, Germany: Springer, 2006.
[34] X. Deng, A. L. Lan, J. Y. Yan, L. Wu, J. Wu, J. J. Zhang, and H. B. Qiu, "Calibrating the amplitude and phase imbalances in AgileDARN HF radar," *Radio Sci.*, vol. 56, no. 5, pp. 1–16, May 2021, doi: 10.1029/2020RS007138.
[35] F. Feng, Y. Li, X. Ye, S. Shi, and S. Li, "Design of radar imaging processing platform based on the architecture with digital signal acquisition board and GPU," in *Proc. 2nd China Int. SAR Symp. (CISS)*, Shanghai, China, 2021, pp. 1–3, doi: 10.23919/CISS51089.2021.9652235.
[36] J. W. Smith and M. Torlak, "Deep-learning-based multiband signal fusion for 3-D SAR superresolution," *IEEE Trans. Aerosp. Electron. Syst.*, vol. 60, no. 1, pp. 8–24, Feb. 2024, doi: 10.1109/TAES.2023.3270111.

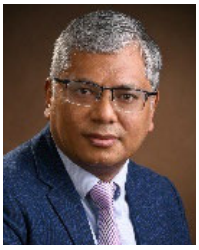

BIKASH NAKARMI (Senior Member, IEEE) received the B.E. degree in electronics and communication, information and communication engineering from Tribhuvan University, Nepal, in 2004, the M.E. degree in electronics and communication, information and communication engineering from Harbin Engineering University, Harbin, China, in 2008, and the Ph.D. degree in electronics and communication, information and communication engineering from Korea Advanced Institute of Science and Technology (KAIST), Daejeon, Republic of Korea, in 2012.

He joined the College of Electronics and Information Engineering, Nanjing University of Aeronautics and Astronautics, China, in 2016, where he is currently a Professor with the Key Laboratory of Radar Imaging and Microwave Photonics, Ministry of Education. From 2012 to 2013, he was the Research and Development Manager of InLC Technology, South Korea. From 2012 to 2014, he was a Postdoctoral Researcher with Nanjing University, China. From 2014 to 2016, he was a Research Professor with KAIST. He has authored and co-authored over 120 research papers, including more than 50 peer-reviewed journal articles in IEEE and OSA, more than 70 international conference papers, and more than 25 keynote and invited talks. His research interests include AI-enabled microwave photonics, interference mitigating, cognitive radar systems, coordinated low altitude economy (LAE) systems, silicon photonics, optical communication and networks using Fabry-Pérot laser diodes, and SPR-based bio-sensors.

Prof. Nakarmi is a Senior Member of OSA, SPIE, and IMS. He has served as a Committee Member for SPIE Photonics Asia 2012, IEEE ICECIT 2021, and IEEE ICECIT 2024. He is an active reviewer for prestigious journals, including Nature, IEEE, and Springer publications.

S. M. REZWANUL ISLAM (Graduate Student Member, IEEE) received the B.Sc. degree in electrical and electronic engineering from Dhaka University of Engineering and Technology (DUET), Gazipur, Bangladesh, in 2021. He is currently pursuing the master's degree in information and communication engineering with the College of Electronics and Information Engineering, Nanjing University of Aeronautics and Astronautics, Nanjing, China. He is focusing on microwave photonics, he generates waveforms, analyzes the interferences, and uses signal processing techniques to solve the issues of photonic radar systems.

HUM NATH PARAJULI (Member, IEEE) received the M.Eng. degree in electrical electronics and information engineering from Osaka University, Osaka, Japan, the M.Sc. degree in photonic networks engineering from Scuola Superiore Sant'Anna, Pisa, Italy, and the Ph.D. degree in electrical engineering from Budapest University of Technology and Economics, Budapest, Hungary. He is currently a Postdoctoral Researcher at Nazarbayev University, Kazakhstan. His current research interests include microwave photonics, deep learning, and adaptive signal processing techniques for optimum waveform design, interference mitigation, and band fusion in radar sensing systems.

IKECHI AUGUSTINE UKAEGBU (Senior Member, IEEE) received the B.Sc. degree in electrical engineering, electromechanics, and electro-technology from Moscow Power Engineering Institute, National Research University, Moscow, Russia, in 2004, the M.Sc. degree in electronics and microelectronics from National Research University, in 2006, and the Ph.D. degree from Korea Advanced Institute of Science and Technology (KAIST), in 2012.

He was a "Brain Korea-21 (BK-21)" Postdoctoral Research Fellow with the Electrical Engineering Department, KAIST, from 2012 to 2013. From 2018 to 2024, he was an Assistant Professor at the Electrical and Computer Engineering Department, School of Engineering and Digital Sciences, Nazarbayev University. Since 2024, he has been an Adjunct Professor at Saint Louis University, St. Louis, MO, USA. He is currently an Assistant Professor with the Division of Engineering Technology, The University of West Alabama, Livingston, AL, USA. In 2018, he founded the Integrated Device Solutions and Nanophotonics (iDSN) Laboratory, Nazarbayev University, where he is the Director. His research interests include circuits and systems, integrated silicon photonics, microwave photonics, optoelectronics, energy harvesting systems, and RF systems. He held research and development positions with the Electronics and Telecommunications Research Institute (ETRI), South Korea, from 2008 to 2009, and Lightron Fiber-Optics Inc., South Korea, in 2013. He was a Senior Engineer with the Design Technology Team, System LSI Division, Samsung Electronics Company Ltd., South Korea, from 2013 to 2016. He co-founded a venture startup company (Axinaux) where he served as the CTO/Product Development Manager, in 2016. He has authored or co-authored over 100 research papers, including 38 peer-reviewed journals and 55 papers in conference proceedings and a book chapter. He is a reviewer of several peer-reviewed journals and has served as a TPC member for several IEEE international conferences.

AIGERIM ASHIMBAYEVA (Graduate Student Member, IEEE) received the B.Eng. and M.Sc. degrees in electrical and electronic engineering from the School of Engineering, Nazarbayev University, in 2015 and 2017, respectively. She is currently pursuing the Ph.D. degree with the Electrical Engineering Program, School of Engineering and Digital Sciences, Nazarbayev University. She is also with the Integrated Device Solutions and Nanophotonics Laboratory. Her research interests include optoelectronics, microwave photonics, interference mitigation in RADARs, and optical signal generation for photonic RADARs.

CARLO MOLARDI (Senior Member, IEEE) received the master's degree in telecommunication engineering and the Ph.D. degree in information technologies from the University of Parma, in 2011 and 2016, respectively, with a focus on numerical methods for optics and electromagnetism, under the supervision of Prof. Stefano Selleri. He is currently an Assistant Professor with the Electrical and Computer Engineering Department, Nazarbayev University, Kazakhstan. Previously, he was a Postdoctoral Researcher with the Information Engineering Department, University of Parma. During his career, he has been awarded several project grants. He is one of the authors of the book *Optical Fiber Biosensors: Device Platforms, Biorecognition, Applications* (Academic Press-Elsevier). His scientific production counts 45 publications in top journals in his area and more than 65 conference proceedings. His research interests include photonic crystal fiber design, fiber lasers for high-power operations, random lasers, fiber optics, fiber sensors, and computational electromagnetism. During the last two years of his Ph.D. period, he was awarded with the prestigious ARAP Scholarship offered by Singapore government, to work as a Research Assistant with Dr. Yu Xia, at Singapore Institute of Manufacturing Technology (SIMTech).

T. D. SUBASH (Senior Member, IEEE) received the B.Eng. degree in electronics and communication engineering, the M.Eng. degree in embedded system technologies, and the Ph.D. degree in nanoelectronics from Anna University, Chennai, India, in 2008, 2011, and 2016, respectively. He is currently a full-time Professor with the School of Marine Engineering Equipment, Zhejiang Ocean University, Zhejiang, China. He is also an Academic Veteran, a Technocrat Cum Avid Researcher, a Mentor, and an Innovation and Entrepreneurship Cell. He enjoys teaching and research. He has 96 publications in international and national journals and 45 papers in international and national conferences in the areas of nanoelectronics, nanoscale device modeling, nanotechnology, and wireless sensor networks. He serves as an active member of the editorial board/ reviewer board of various international journals. He is serving on the Board of Governors, IEEE Photonics Society, USA. He is also the Founding Chairperson of the IEEE Photonics Society Madras Chapter, until 2020.

XIANGCHUAN WANG received the B.Eng. degree in automation and the Ph.D. degree in microelectronics and solid-state electronics from Nanjing University, Nanjing, China, in 2009 and 2015, respectively. He is currently a Research Professor with the Key Laboratory of Radar Imaging and Microwave Photonics, Ministry of Education, Nanjing University of Aeronautics and Astronautics, Nanjing. He has authored and co-authored over 70 research articles. His current research interests include microwave photonics measurement and radar imaging.

SHILONG PAN (Fellow, IEEE) received the B.S. and Ph.D. degrees in electronic engineering from Tsinghua University, Beijing, China, in 2004 and 2008, respectively.

From 2008 to 2010, he was a "Vision 2010" Postdoctoral Research Fellow with the Microwave Photonics Research Laboratory, University of Ottawa, Ottawa, ON, Canada. In 2010, he joined the College of Electronic and Information Engineering, Nanjing University of Aeronautics and Astronautics, Nanjing, China, where he is currently a Full Professor and the Director of the National Key Laboratory of Microwave Photonics. He has authored or co-authored over 400 research articles, including more than 250 papers in peer-reviewed journals and 150 papers in conference proceedings. His research focused on microwave photonics, which includes optical generation and processing of microwave signals, ultra-wideband over fiber, photonic microwave measurement, and integrated microwave photonics.

Prof. Pan is a fellow of the IEEE Microwave Theory and Techniques Society, the IEEE Photonics Society, the IEEE Instrumentation and Measurement Society, and the Optical Society of America. He was selected to receive an OSA Outstanding Reviewer Award, in 2015. He was the Chair of numerous international conferences and workshops, including the TPC Chair of IEEE ICOCN 2015; the TPC Chair of the High-Speed and Broadband Wireless Technologies Subcommittee of the IEEE Radio Wireless Symposium, in 2013, 2014, and 2016; the TPC Chair of the Optical Fiber Sensors and Microwave Photonics Subcommittee Chair of the Opto-Electronics and Communication Conference, in 2015; the Chair of the Microwave Photonics for Broadband Measurement Workshop of International Microwave Symposium in 2015; the TPC Chair of the microwave photonics subcommittee of CLEO-PR, OECC, and PGC 2017 (joint conference); and the TPC Co-Chair of IEEE MWP 2017. He is currently a Topical Editor of *Chinese Optics Letters*.